Radio-frequency spectroscopy of weakly bound molecules in spin-orbit-coupled atomic Fermi gases

Hui Hu,[1] Han Pu,[2] Jing Zhang,[3] Shi-Guo Peng,[4] and Xia-Ji Liu[1,*]

[1]*ARC Centre of Excellence for Quantum-Atom Optics and Centre for Atom Optics and Ultrafast Spectroscopy, Swinburne University of Technology, Melbourne 3122, Australia*

[2]*Department of Physics and Astronomy and Rice Quantum Institute, Rice University, Houston, Texas 77251, USA*

[3]*State Key Laboratory of Quantum Optics and Quantum Optics Devices, Institute of Opto-Electronics, Shanxi University, Taiyuan 030006, People's Republic of China*

[4]*State Key Laboratory of Magnetic Resonance and Atomic and Molecular Physics, Wuhan Institute of Physics and Mathematics, Chinese Academy of Sciences, Wuhan 430071, People's Republic of China*

(Received 23 June 2012; published 27 November 2012)

We investigate theoretically radio-frequency spectroscopy of weakly bound molecules in an ultracold spin-orbit-coupled atomic Fermi gas. We consider two cases with either equal Rashba and Dresselhaus coupling or pure Rashba coupling. The former system has been realized very recently at Shanxi University [Wang *et al.*, Phys. Rev. Lett. **109**, 095301 (2012)] and MIT [Cheuk *et al.*, Phys. Rev. Lett. **109**, 095302 (2012)]. We predict realistic radio-frequency signals for revealing the unique properties of anisotropic molecules formed by spin-orbit coupling.

DOI: 10.1103/PhysRevA.86.053627 PACS number(s): 03.75.Ss, 03.75.Hh, 05.30.Fk, 67.85.−d

I. INTRODUCTION

The coupling between the spin of electrons to their orbital motion, the so-called spin-orbit coupling, lies at the heart of a variety of intriguing phenomena in diverse fields of physics. It is responsible for the well-known fine structure of atomic spectra in atomic physics, as well as the recently discovered topological state of matter in solid-state physics, such as topological insulators and superconductors [1,2]. For electrons, spin-orbit coupling is a relativistic effect and, in general, not strong. Most recently, in a milestone experiment at the National Institute of Standards and Technology (NIST), synthetic spin-orbit coupling was created and detected in an atomic Bose-Einstein condensate (BEC) of ^{87}Rb atoms [3]. Using the same experimental technique, noninteracting spin-orbit-coupled Fermi gases of ^{40}K atoms and ^{6}Li atoms have also been realized, respectively, at Shanxi University [4] and at Massachusetts Institute of Technology (MIT) [5]. These experiments have paved an entirely new way to investigate the celebrated effects of spin-orbit coupling.

Owing to the high controllability of ultracold atoms in atomic species, interactions, confining geometry and purity, the advantage of using synthetic spin-orbit coupling is apparent: (i) The strength of spin-orbit coupling between ultracold atoms can be made very strong, much stronger than that in solids. (ii) New bosonic topological states that have no analogy in solid-state systems may be created. (iii) Ultracold atoms are able to realize topological superfluids that are yet to be observed in the solid state. (iv) Strongly correlated topological states can be readily realized, whose understanding remains a grand challenge. At the moment, there has been a flood of theoretical work on synthetic spin-orbit coupling in BECs [6–18] and atomic Fermi gases [19–31], addressing particularly new exotic superfluid phases arising from spin-orbit coupling [8,9,13,23].

In this paper, we investigate theoretically momentum-resolved radio-frequency (rf) spectroscopy of an *interacting* two-component atomic Fermi gas with spin-orbit coupling. The interatomic interactions can be easily manipulated using a Feshbach resonance in ^{40}K or ^{6}Li atoms [32]. In our previous work, we have shown that weakly bound molecules with anisotropic mass and anisotropic wave function (in momentum space) may be formed due to spin-orbit coupling [23] (see also the work in Refs. [19,22]). Here, we aim to predict observable rf signals of these anisotropic molecules, using the known two-particle wave function [22]. Our calculation is based on Fermi's golden rule for the bound-free transition of a stationary molecule [33]. We consider two kinds of spin-orbit coupling: (1) the equal Rashba and Dresselhaus coupling $\lambda k_x \sigma_y$, which has been realized experimentally at Shanxi University [4] and MIT [5], and (2) the pure Rashba coupling $\lambda(k_y\sigma_x - k_x\sigma_y)$, which is yet to be realized. Here σ_x and σ_y are the Pauli matrices, k_x and k_y are momenta, and λ is the strength of the spin-orbit coupling. The latter case with pure Rashba spin-orbit coupling is of particular theoretical interest, since molecules induced by spin-orbit coupling exist even for a negative s-wave scattering length above Feshbach resonances [19,22,23].

Explicitly we calculate the molecular response in the radio-frequency spectroscopy. These results should be quantitatively reliable in the deep BEC limit with negligible number of atoms, i.e., in the interaction parameter regime with $1/(k_F a_s) > 2$, where k_F and a_s are the Fermi wavelength and s-wave scattering length, respectively. However, in a real experiment, in order to maximize the spin-orbit effect, it is better to work closer to Feshbach resonances, i.e., $1/(k_F a_s) \sim 0.5$. Moreover, the typical temperature in experiment is about $0.6T_F$, where T_F is the Fermi temperature. Thus, at finite temperatures the spin-orbit-coupled Fermi gas consists of both atoms and weakly bound molecules, which may strongly interact with each other. Our prediction for the molecular response is still qualitatively valid, with the understanding that there would be an additional pronounced atomic response in the rf spectra.

The paper is structured as follows. In the next section, we discuss briefly the rf spectroscopy and Fermi's golden rule for the calculation of rf transfer strength. In Sec. III, we consider the experimental case of equal Rashba and Dresselhaus spin-orbit coupling. We introduce first the model Hamiltonian

*xiajiliu@swin.edu.au

and the single-particle and two-particle wave functions. We then derive an analytic expression for momentum-resolved rf transfer strength following Fermi's golden rule. It can be written explicitly in terms of the two-body wave function. We discuss in detail the distinct features of momentum-resolved rf spectroscopy in the presence of spin-orbit coupling, with the use of realistic experimental parameters. In Sec. IV, we consider an atomic Fermi gas with pure Rashba spin-orbit coupling, a system anticipated to be realized in the near future. Finally, in Sec. V, we conclude and make some final remarks.

II. RADIO-FREQUENCY SPECTROSCOPY AND FERMI'S GOLDEN RULE

Radio-frequency spectroscopy, including momentum-resolved rf spectroscopy, is a powerful tool to characterize interacting many-body systems. It has been widely used to study fermionic pairing in a two-component atomic Fermi gas near Feshbach resonances when it crosses from a Bardeen-Cooper-Schrieffer (BCS) superfluid of weakly interacting Cooper pairs into a BEC of tightly bound molecules [34–36]. Most recently, it has also been used to detect new quasiparticles known as repulsive polarons [37,38], which occur when "impurity" fermionic particles interact repulsively with a fermionic environment.

The underlying mechanics of rf spectroscopy is simple. For an atomic Fermi gas with two hyperfine states, denoted as $|1\rangle = |\uparrow\rangle$ and $|2\rangle = |\downarrow\rangle$, the rf field drives transitions between one of the hyperfine states (i.e., $|\downarrow\rangle$) and an empty hyperfine state $|3\rangle$ which lies above it by an energy $\hbar\omega_{3\downarrow}$ due to the magnetic field splitting in bare atomic hyperfine levels. The Hamiltonian for rf coupling may be written as

$$\mathcal{V}_{\rm rf} = V_0 \int d\mathbf{r}[\psi_3^\dagger(\mathbf{r})\,\psi_\downarrow(\mathbf{r}) + \psi_\downarrow^\dagger(\mathbf{r})\,\psi_3(\mathbf{r})], \qquad (1)$$

where $\psi_3^\dagger(\mathbf{r})$ $[\psi_\downarrow^\dagger(\mathbf{r})]$ is the field operator which creates an atom in $|3\rangle$ $(|\downarrow\rangle)$ at the position $\mathbf{r}$, and V_0 is the strength of the rf drive and is related to the Rabi frequency ω_R with $V_0 = \hbar\omega_R/2$.

For the rf spectroscopy of weakly bound molecules that is of interest in this work, a molecule is initially at rest in the bound state $|\Phi_{2B}\rangle$ with energy $E_0 = -\epsilon_B$. Here ϵ_B is the binding energy of the molecules. A radio-frequency photon with energy $\hbar\omega$ will break the molecule and transfer one of the atoms to the third state $|3\rangle$. In the case that there is no interaction between the state $|3\rangle$ and the spin-up and spin-down states, the final state $|\Phi_f\rangle$ involves a free atom in the third state and a remaining atom in the system. According to Fermi's golden rule, the rf strength of breaking molecules and transferring atoms is proportional to the Franck-Condon factor [33]

$$F(\omega) = |\langle\Phi_f|\mathcal{V}_{\rm rf}|\Phi_{2B}\rangle|^2\delta\left[\omega - \omega_{3\downarrow} - \frac{E_f - E_0}{\hbar}\right], \qquad (2)$$

where the Dirac δ function ensures energy conservation and E_f is the energy of the final state. The integrated Franck-Condon factor over frequency should be unity $\int_{-\infty}^{+\infty} F(\omega)\,d\omega = 1$, if we can find a complete set of final states for rf transition. Hereafter, without any confusion we shall ignore the energy splitting in the bare atomic hyperfine levels and set $\omega_{3\downarrow} = 0$. To calculate the Franck-Condon factor Eq. (2), it is crucial to understand the initial two-particle bound state $|\Phi_{2B}\rangle$ and the final two-particle state $|\Phi_f\rangle$.

III. EQUAL RASHBA AND DRESSELHAUS SPIN-ORBIT COUPLING

Let us first consider a spin-orbit-coupled atomic Fermi gas realized recently at Shanxi University [4] and at MIT [5]. In these two experiments, the spin-orbit coupling is induced by the spatial dependence of two counterpropagating Raman laser beams that couple the two spin states of the system. Near Feshbach resonances, the system may be described by a model Hamiltonian $\mathcal{H} = \mathcal{H}_0 + \mathcal{H}_{\rm int}$, where

$$\mathcal{H}_0 = \sum_\sigma \int d\mathbf{r}\,\psi_\sigma^\dagger(\mathbf{r})\frac{\hbar^2\hat{\mathbf{k}}^2}{2m}\psi_\sigma(\mathbf{r}) + \int d\mathbf{r}\left[\psi_\uparrow^\dagger(\mathbf{r})\left(\frac{\Omega_R}{2}e^{i2k_Rx}\right)\psi_\downarrow(\mathbf{r}) + \text{H.c.}\right] \qquad (3)$$

is the single-particle Hamiltonian and

$$\mathcal{H}_{\rm int} = U_0 \int d\mathbf{r}\,\psi_\uparrow^\dagger(\mathbf{r})\,\psi_\downarrow^\dagger(\mathbf{r})\,\psi_\downarrow(\mathbf{r})\,\psi_\uparrow(\mathbf{r}) \qquad (4)$$

is the interaction Hamiltonian describing the contact interaction between two spin states. Here, $\psi_\sigma^\dagger(\mathbf{r})$ is the creation field operator for atoms in the spin state σ, $\hbar\hat{\mathbf{k}} \equiv -i\hbar\nabla$ is the momentum operator, Ω_R is the coupling strength of Raman beams, $k_R = 2\pi/\lambda_R$ is determined by the wavelength λ_R of two Raman lasers, and therefore $2\hbar k_R$ is the momentum transfer during the two-photon Raman process. The interaction strength is denoted by the bare interaction parameter U_0. It should be regularized in terms of the s-wave scattering length a_s, i.e., $1/U_0 = m/(4\pi\hbar^2 a_s) - \sum_{\mathbf{k}} m/(\hbar^2\mathbf{k}^2)$.

To solve the many-body Hamiltonian equation (3), it is useful to remove the spatial dependence of the Raman coupling term, by introducing the following new field operators $\tilde{\psi}_\sigma$ via

$$\psi_\uparrow(\mathbf{r}) = e^{+ik_Rx}\tilde{\psi}_\uparrow(\mathbf{r}), \qquad (5)$$

$$\psi_\downarrow(\mathbf{r}) = e^{-ik_Rx}\tilde{\psi}_\downarrow(\mathbf{r}). \qquad (6)$$

With the new field operators $\tilde{\psi}_\sigma$, the single-particle Hamiltonian then becomes

$$\mathcal{H}_0 = \sum_\sigma \int d\mathbf{r}\,\tilde{\psi}_\sigma^\dagger(\mathbf{r})\frac{\hbar^2(\hat{\mathbf{k}} \pm k_R\mathbf{e}_x)^2}{2m}\tilde{\psi}_\sigma(\mathbf{r}) + \frac{\Omega_R}{2}\int d\mathbf{r}[\tilde{\psi}_\uparrow^\dagger(\mathbf{r})\,\tilde{\psi}_\downarrow(\mathbf{r}) + \text{H.c.}], \qquad (7)$$

where in the first term on the right-hand side of the equation we take "+" for spin-up atoms and "−" for spin-down atoms. The form of the interaction Hamiltonian is invariant:

$$\mathcal{H}_{\rm int} = U_0 \int d\mathbf{r}\,\tilde{\psi}_\uparrow^\dagger(\mathbf{r})\,\tilde{\psi}_\downarrow^\dagger(\mathbf{r})\,\tilde{\psi}_\downarrow(\mathbf{r})\,\tilde{\psi}_\uparrow(\mathbf{r}). \qquad (8)$$

However, the rf Hamiltonian acquires an effective momentum transfer $k_R\mathbf{e}_x$,

$$\mathcal{V}_{\rm rf} = V_0 \int d\mathbf{r}[e^{-ik_Rx}\psi_3^\dagger(\mathbf{r})\,\tilde{\psi}_\downarrow(\mathbf{r}) + \text{H.c.}]. \qquad (9)$$

For later reference, we shall rewrite the rf Hamiltonian in terms of field operators in the momentum space,

$$\mathcal{V}_{\rm rf} = V_0 \sum_{\mathbf{q}} (c^\dagger_{\mathbf{q}-k_R\mathbf{e}_x,3} c_{\mathbf{q}\downarrow} + \text{H.c.}), \tag{10}$$

where $\psi_3^\dagger(\mathbf{r}) \equiv \sum_{\mathbf{q}} c^\dagger_{\mathbf{q}3} e^{i\mathbf{q}\cdot\mathbf{r}}$ and $\tilde{\psi}_\downarrow(\mathbf{r}) \equiv \sum_{\mathbf{q}} c_{\mathbf{q}\downarrow} e^{i\mathbf{q}\cdot\mathbf{r}}$. Hereafter, we shall denote $c_{\mathbf{k}3}$ and $c_{\mathbf{k}\sigma}$ as the field operators (in the momentum space) for atoms in the third state and in the spin state σ, respectively.

A. Single-particle solution

Using the Pauli matrices, the single-particle Hamiltonian takes the form

$$\mathcal{H}_0 = \int d\mathbf{r}[\tilde{\psi}^\dagger_\uparrow(\mathbf{r}), \tilde{\psi}^\dagger_\downarrow(\mathbf{r})] \times \left[\frac{\hbar^2(k_R^2 + k^2)}{2m} + h\sigma_x + \lambda k_x \sigma_z\right] \begin{bmatrix} \tilde{\psi}_\uparrow(\mathbf{r}) \\ \tilde{\psi}_\downarrow(\mathbf{r}) \end{bmatrix}, \tag{11}$$

where for convenience we have defined the spin-orbit coupling constant denoted as $\lambda \equiv \hbar^2 k_R/m$ and an "effective" Zeeman field $h \equiv \Omega_R/2$. This Hamiltonian is equivalent to the one with equal Rashba and Dresselhaus spin-orbit coupling, $\lambda k_x \sigma_y$. To see this, let us take the second transformation and introduce new field operators $\Psi_\sigma(\mathbf{r})$ via

$$\tilde{\psi}_\uparrow(\mathbf{r}) = \frac{1}{\sqrt{2}}[\Psi_\uparrow(\mathbf{r}) - i\Psi_\downarrow(\mathbf{r})], \tag{12}$$

$$\tilde{\psi}_\downarrow(\mathbf{r}) = \frac{1}{\sqrt{2}}[\Psi_\uparrow(\mathbf{r}) + i\Psi_\downarrow(\mathbf{r})]. \tag{13}$$

Using these new field operators, the single-particle Hamiltonian now takes the form

$$\mathcal{H}_0 = \int d\mathbf{r}[\Psi^\dagger_\uparrow(\mathbf{r}), \Psi^\dagger_\downarrow(\mathbf{r})] \times \left[\frac{\hbar^2(k_R^2 + k^2)}{2m} + \lambda k_x \sigma_y + h\sigma_z\right] \begin{bmatrix} \Psi_\uparrow(\mathbf{r}) \\ \Psi_\downarrow(\mathbf{r}) \end{bmatrix}, \tag{14}$$

which is precisely the Hamiltonian with equal Rashba and Dresselhaus spin-orbit coupling.

The single-particle Hamiltonian equation (11) can be diagonalized to yield two eigenvalues:

$$E_{\mathbf{k}\pm} = \frac{\hbar^2 k_R^2}{2m} + \frac{\hbar^2 k^2}{2m} \pm \sqrt{h^2 + \lambda^2 k_x^2}. \tag{15}$$

Here "±" stands for the two helicity branches. The single-particle eigenstates or the field operators in the helicity basis take the form

$$c_{\mathbf{k}+} = +c_{\mathbf{k}\uparrow}\cos\theta_{\mathbf{k}} + c_{\mathbf{k}\downarrow}\sin\theta_{\mathbf{k}}, \tag{16}$$

$$c_{\mathbf{k}-} = -c_{\mathbf{k}\uparrow}\sin\theta_{\mathbf{k}} + c_{\mathbf{k}\downarrow}\cos\theta_{\mathbf{k}}, \tag{17}$$

where

$$\theta_{\mathbf{k}} = \arctan\left[(\sqrt{h^2 + \lambda^2 k_x^2} - \lambda k_x)/h\right] > 0 \tag{18}$$

is an angle determined by h and k_x. Note that,

$$\cos^2\theta_{\mathbf{k}} = \frac{1}{2}\left(1 + \frac{\lambda k_x}{\sqrt{h^2 + \lambda^2 k_x^2}}\right), \tag{19}$$

$$\sin^2\theta_{\mathbf{k}} = \frac{1}{2}\left(1 - \frac{\lambda k_x}{\sqrt{h^2 + \lambda^2 k_x^2}}\right). \tag{20}$$

Note also that the minimum energy of the single-particle energy dispersion is given by [24]

$$E_{\rm min} = \frac{\hbar^2 k_R^2}{2m} - \frac{m\lambda^2}{2\hbar^2} - \frac{\hbar^2 h^2}{2m\lambda^2} = -\frac{\hbar^2 h^2}{2m\lambda^2}, \tag{21}$$

if $h < m\lambda^2/\hbar^2$.

B. The initial two-particle bound state $|\Phi_{2B}\rangle$

In the presence of spin-orbit coupling, the wave function of the initial two-body bound state has both spin-singlet and -triplet components [19,22,23]. For the Rashba spin-orbit coupling, the two-body wave function has been explicitly constructed by Yu and Zhai [22]. Here, we apply their construction to the case with equal Rashba and Dresselhaus spin-orbit coupling. The wave function at zero center-of-mass momentum $|\Phi_{2B}\rangle$ may be written as [22]

$$|\Phi_{2B}\rangle = \frac{1}{\sqrt{2\mathcal{C}}}\sum_{\mathbf{k}}[\psi_{\uparrow\downarrow}(\mathbf{k})c^\dagger_{\mathbf{k}\uparrow}c^\dagger_{-\mathbf{k}\downarrow} + \psi_{\downarrow\uparrow}(\mathbf{k})c^\dagger_{\mathbf{k}\downarrow}c^\dagger_{-\mathbf{k}\uparrow} + \psi_{\uparrow\uparrow}(\mathbf{k})c^\dagger_{\mathbf{k}\uparrow}c^\dagger_{-\mathbf{k}\uparrow} + \psi_{\downarrow\downarrow}(\mathbf{k})c^\dagger_{\mathbf{k}\downarrow}c^\dagger_{-\mathbf{k}\downarrow}]|\text{vac}\rangle, \tag{22}$$

where $c^\dagger_{\mathbf{k}\uparrow}$ and $c^\dagger_{\mathbf{k}\downarrow}$ are creation field operators of spin-up and spin-down atoms with momentum $\mathbf{k}$, and $\mathcal{C} \equiv \sum_{\mathbf{k}}[|\psi_{\uparrow\downarrow}(\mathbf{k})|^2 + |\psi_{\downarrow\uparrow}(\mathbf{k})|^2 + |\psi_{\uparrow\uparrow}(\mathbf{k})|^2 + |\psi_{\downarrow\downarrow}(\mathbf{k})|^2]$ is the normalization factor. From the Schrödinger equation $(\mathcal{H}_0 + \mathcal{H}_{\rm int})|\Phi_{2B}\rangle = E_0|\Phi_{2B}\rangle$, we can straightforwardly derive the following equations for coefficients $\psi_{\sigma\sigma'}$ appearing in the above two-body wave function [22]:

$$\left[E_0 - \left(\frac{\hbar^2 k_R^2}{m} + \frac{\hbar^2 k^2}{m} + 2\lambda k_x\right)\right]\psi_{\uparrow\downarrow}(\mathbf{k}) = +\frac{U_0}{2}\sum_{\mathbf{k}'}[\psi_{\uparrow\downarrow}(\mathbf{k}') - \psi_{\downarrow\uparrow}(\mathbf{k}')] + h\psi_{\uparrow\uparrow}(\mathbf{k}) + h\psi_{\downarrow\downarrow}(\mathbf{k}), \tag{23}$$

$$\left[E_0 - \left(\frac{\hbar^2 k_R^2}{m} + \frac{\hbar^2 k^2}{m} - 2\lambda k_x\right)\right]\psi_{\downarrow\uparrow}(\mathbf{k}) = -\frac{U_0}{2}\sum_{\mathbf{k}'}[\psi_{\uparrow\downarrow}(\mathbf{k}') - \psi_{\downarrow\uparrow}(\mathbf{k}')] + h\psi_{\uparrow\uparrow}(\mathbf{k}) + h\psi_{\downarrow\downarrow}(\mathbf{k}), \tag{24}$$

$$\left[E_0 - \left(\frac{\hbar^2 k_R^2}{m} + \frac{\hbar^2 k^2}{m}\right)\right]\psi_{\uparrow\uparrow}(\mathbf{k}) = h\psi_{\uparrow\downarrow}(\mathbf{k}) + h\psi_{\downarrow\uparrow}(\mathbf{k}), \tag{25}$$

$$\left[E_0 - \left(\frac{\hbar^2 k_R^2}{m} + \frac{\hbar^2 k^2}{m}\right)\right]\psi_{\downarrow\downarrow}(\mathbf{k}) = h\psi_{\uparrow\downarrow}(\mathbf{k}) + h\psi_{\downarrow\uparrow}(\mathbf{k}), \tag{26}$$

where $E_0 = -\epsilon_B < 0$ is the energy of the two-body bound state. Let us introduce $A_{\mathbf{k}} \equiv -\epsilon_B - (\hbar^2 k_R^2/m + \hbar^2 k^2/m) < 0$ and different spin components of the wave functions,

$$\psi_s(\mathbf{k}) = \frac{1}{\sqrt{2}}[\psi_{\uparrow\downarrow}(\mathbf{k}) - \psi_{\downarrow\uparrow}(\mathbf{k})], \tag{27}$$

$$\psi_a(\mathbf{k}) = \frac{1}{\sqrt{2}}[\psi_{\uparrow\downarrow}(\mathbf{k}) + \psi_{\downarrow\uparrow}(\mathbf{k})]. \tag{28}$$

It is easy to see that

$$\psi_{\uparrow\uparrow}(\mathbf{k}) = \frac{\sqrt{2}h}{A_{\mathbf{k}}}\psi_a(\mathbf{k}), \tag{29}$$

$$\psi_{\downarrow\downarrow}(\mathbf{k}) = \frac{\sqrt{2}h}{A_{\mathbf{k}}}\psi_a(\mathbf{k}), \tag{30}$$

$$\psi_a(\mathbf{k}) = \lambda k_x \left[\frac{1}{A_{\mathbf{k}} - 2h} + \frac{1}{A_{\mathbf{k}} + 2h}\right]\psi_s(\mathbf{k}), \tag{31}$$

and

$$\left[A_{\mathbf{k}} - \frac{4\lambda^2 k_x^2}{A_{\mathbf{k}} - 4h^2/A_{\mathbf{k}}}\right]\psi_s(\mathbf{k}) = U_0 \sum_{\mathbf{k}'} \psi_s(\mathbf{k}'). \tag{32}$$

As required by the symmetry of fermionic systems, the spin-singlet wave function $\psi_s(\mathbf{k})$ is an even function of the momentum $\mathbf{k}$, i.e., $\psi_s(-\mathbf{k}) = \psi_s(\mathbf{k})$, and the spin-triplet wave functions are odd functions, satisfying $\psi_a(-\mathbf{k}) = -\psi_a(\mathbf{k})$, $\psi_{\uparrow\uparrow}(-\mathbf{k}) = -\psi_{\uparrow\uparrow}(\mathbf{k})$, and $\psi_{\downarrow\downarrow}(-\mathbf{k}) = -\psi_{\downarrow\downarrow}(\mathbf{k})$. The un-normalized wave function $\psi_s(\mathbf{k}) = [A_{\mathbf{k}} - 4\lambda^2 k_x^2/(A_{\mathbf{k}} - 4h^2/A_{\mathbf{k}})]^{-1}$ is given by

$$\psi_s(\mathbf{k}) = \frac{1}{h^2 + \lambda^2 k_x^2}\left[\frac{h^2}{A_{\mathbf{k}}} + \frac{\lambda^2 k_x^2 A_{\mathbf{k}}}{A_{\mathbf{k}}^2 - 4\left(h^2 + \lambda^2 k_x^2\right)}\right]. \tag{33}$$

Using Eq. (32) and un-normalized wave function $\psi_s(\mathbf{k})$, the bound-state energy E_0 or the binding energy ϵ_B is determined by $U_0 \sum_{\mathbf{k}} \psi_s(\mathbf{k}) = 1$, or more explicitly,

$$\frac{m}{4\pi\hbar^2 a_s} - \sum_{\mathbf{k}}\left[\psi_s(\mathbf{k}) + \frac{m}{\hbar^2 k^2}\right] = 0. \tag{34}$$

Here we have replaced the bare interaction strength U_0 by the s-wave scattering length a_s using the standard regularization scheme mentioned earlier. The normalization factor of the total two-body wave function is given by

$$\mathcal{C} = \sum_{\mathbf{k}} |\psi_s(\mathbf{k})|^2 \left[1 + \frac{2\lambda^2 k_x^2}{(A_{\mathbf{k}} - 2h)^2} + \frac{2\lambda^2 k_x^2}{(A_{\mathbf{k}} + 2h)^2}\right]. \tag{35}$$

C. The final two-particle state $|\Phi_f\rangle$

Let us consider now the final state $|\Phi_f\rangle$. For this purpose, it is useful to calculate

$$\mathcal{V}_{\mathrm{rf}}|\Phi_{2B}\rangle = V_0 \sum_{\mathbf{q}} c^\dagger_{-\mathbf{q}-k_R\mathbf{e}_x,3} c_{-\mathbf{q}\downarrow}|\Phi_{2B}\rangle \tag{36}$$

and then determine possible final states. It can be readily seen that

$$\mathcal{V}_{\mathrm{rf}}|\Phi_{2B}\rangle = -\frac{V_0}{\sqrt{2\mathcal{C}}} \sum_{\mathbf{q}} c^\dagger_{-\mathbf{q}-k_R\mathbf{e}_x,3}\{[\psi_{\uparrow\downarrow}(\mathbf{q}) - \psi_{\downarrow\uparrow}(-\mathbf{q})]c^\dagger_{\mathbf{q}\uparrow} + [\psi_{\downarrow\downarrow}(\mathbf{q}) - \psi_{\downarrow\downarrow}(-\mathbf{q})]c^\dagger_{\mathbf{q}\downarrow}\}|\mathrm{vac}\rangle. \tag{37}$$

Rewriting $\psi_{\uparrow\downarrow}$ and $\psi_{\downarrow\uparrow}$ in terms of ψ_s and ψ_a as shown in Eqs. (27) and (28), and exploiting the parity of the wave functions, we obtain a general result valid for any type of spin-orbit coupling,

$$\mathcal{V}_{\mathrm{rf}}|\Phi_{2B}\rangle = -\sqrt{\frac{1}{\mathcal{C}}} V_0 \sum_{\mathbf{q}} c^\dagger_{-\mathbf{q}-k_R\mathbf{e}_x,3}\{[\psi_s(\mathbf{q}) + \psi_a(\mathbf{q})]c^\dagger_{\mathbf{q}\uparrow} + \sqrt{2}\psi_{\downarrow\downarrow}(\mathbf{q})c^\dagger_{\mathbf{q}\downarrow}\}|\mathrm{vac}\rangle. \tag{38}$$

To proceed, we need to rewrite the field operators $c^\dagger_{\mathbf{q}\uparrow}$ and $c^\dagger_{\mathbf{q}\downarrow}$ in terms of creation operators in the helicity basis. For the case of equal Rashba and Dresselhaus spin-orbit coupling, using Eqs. (16) and (17), we find that

$$c^\dagger_{\mathbf{q}\uparrow} = \cos\theta_{\mathbf{q}} c^\dagger_{\mathbf{q}+} - \sin\theta_{\mathbf{q}} c^\dagger_{\mathbf{q}-}, \tag{39}$$

$$c^\dagger_{\mathbf{q}\downarrow} = \sin\theta_{\mathbf{q}} c^\dagger_{\mathbf{q}+} + \cos\theta_{\mathbf{q}} c^\dagger_{\mathbf{q}-}. \tag{40}$$

Thus, we obtain

$$\mathcal{V}_{\mathrm{rf}}|\Phi_{2B}\rangle = -\sqrt{\frac{1}{\mathcal{C}}} V_0 \sum_{\mathbf{q}} c^\dagger_{-\mathbf{q}-k_R\mathbf{e}_x,3}[s_{\mathbf{q}+}c^\dagger_{\mathbf{q}+} - s_{\mathbf{q}-}c^\dagger_{\mathbf{q}-}]|\mathrm{vac}\rangle, \tag{41}$$

where

$$s_{\mathbf{q}+} = [\psi_s(\mathbf{q}) + \psi_a(\mathbf{q})]\cos\theta_{\mathbf{q}} + \sqrt{2}\psi_{\downarrow\downarrow}(\mathbf{q})\sin\theta_{\mathbf{q}}, \tag{42}$$

$$s_{\mathbf{q}-} = [\psi_s(\mathbf{q}) + \psi_a(\mathbf{q})]\sin\theta_{\mathbf{q}} - \sqrt{2}\psi_{\downarrow\downarrow}(\mathbf{q})\cos\theta_{\mathbf{q}}. \tag{43}$$

Equation (41) can be interpreted as follows. The rf photon breaks a stationary molecule and transfers a spin-down atom to the third state. We have two possible final states: (1) we may have two atoms in the third state and the upper helicity state, respectively, with a possibility of $|s_{\mathbf{q}+}|^2/\mathcal{C}$; and (2) we may also have a possibility of $|s_{\mathbf{q}-}|^2/\mathcal{C}$ for having two atoms in the third state and the lower helicity state, respectively.

D. Momentum-resolved rf spectroscopy

Taking into account these two final states and using Fermi's golden rule, we end up with the following expression for the Franck-Condon factor:

$$F(\omega) = \frac{1}{\mathcal{C}}\sum_{\mathbf{q}}\left[s^2_{\mathbf{q}+}\delta\left(\omega - \frac{\mathcal{E}_{\mathbf{q}+}}{\hbar}\right) + s^2_{\mathbf{q}-}\delta\left(\omega - \frac{\mathcal{E}_{\mathbf{q}-}}{\hbar}\right)\right], \tag{44}$$

where

$$\mathcal{E}_{\mathbf{q}\pm} \equiv \epsilon_B + \frac{\hbar^2\left(k_R^2 + q^2\right)}{2m} \pm \sqrt{h^2 + \lambda^2 q_x^2} + \frac{\hbar^2(\mathbf{q} + k_R\mathbf{e}_x)^2}{2m}. \tag{45}$$

The two Dirac δ functions in Eq. (44) are due to energy conservation. For example, the energy of the initial state (of the stationary molecule) is $E_0 = -\epsilon_B$, while the energy of the final state is $\hbar^2(\mathbf{q} + k_R\mathbf{e}_x)^2/(2m)$ for the free atom in the third state and $\hbar^2(k_R^2 + q^2)/(2m) + \sqrt{h^2 + \lambda^2 q_x^2}$ for the remaining atom in the upper branch. Therefore, the rf energy $\hbar\omega$ required to have such a transfer is given by $\mathcal{E}_{\mathbf{q}+}$, as shown by the first Dirac δ function. It is easy to check that the Franck-Condon factor is integrated to unity, $\int_{-\infty}^{+\infty} F(\omega) = 1$.

Experimentally, in addition to measuring the total number of atoms transferred to the third state, which is proportional to $F(\omega)$, we may also resolve the transferred number of atoms for a given momentum or wave vector k_x. Such a momentum-resolved rf spectroscopy has already been implemented for a noninteracting spin-orbit-coupled atomic Fermi gas at Shanxi University and at MIT. Accordingly, we may define a momentum-resolved Franck-Condon factor

$$F(k_x,\omega) = \frac{1}{\mathcal{C}}\sum_{\mathbf{q}_\perp}\left[s_{\mathbf{q}+}^2\,\delta\left(\omega - \frac{\mathcal{E}_{\mathbf{q}+}}{\hbar}\right) + s_{\mathbf{q}-}^2\,\delta\left(\omega - \frac{\mathcal{E}_{\mathbf{q}-}}{\hbar}\right)\right], \tag{46}$$

where the summations are now over the wave vector $\mathbf{q}_\perp \equiv (q_y,q_z)$ and we have defined $k_x \equiv q_x + k_R$ by shifting the wave vector q_x by an amount k_R. This shift is due to the gauge transformation used in Eqs. (5) and (6). With the help of the two Dirac δ functions, the summation over $\mathbf{q}_\perp$ may be done analytically. We finally arrive at

$$F(k_x,\omega) = \frac{m}{8\pi^2\hbar\mathcal{C}}\left[s_{\mathbf{q}+}^2\,\Theta(q_{\perp,+}^2) + s_{\mathbf{q}-}^2\,\Theta(q_{\perp,-}^2)\right], \tag{47}$$

where $\Theta(x)$ is the step function and

$$q_{\perp,\pm}^2 = \frac{m}{\hbar}\left(\omega - \frac{\epsilon_B}{\hbar}\right) - \left(k_R^2 + q_x^2 + q_x k_R \pm \frac{m}{\hbar^2}\sqrt{h^2+\lambda^2 q_x^2}\right). \tag{48}$$

It is understood that we will use $\mathbf{q} = (q_x,q_{\perp,+})$ in the calculation of $s_{\mathbf{q}+}$ and $\mathbf{q} = (q_x,q_{\perp,-})$ in $s_{\mathbf{q}-}$.

We may immediately realize from the above expression that the momentum-resolved Franck-Condon factor is an asymmetric function of k_x, due to the coexistence of spin-singlet and spin-triplet wave functions in the initial two-body bound state. Moreover, the contribution from two final states or two branches should manifest themselves in the different frequency domain in rf spectra. As we shall see below, these features give us clear signals of anisotropic bound molecules formed by spin-orbit coupling. On the other hand, from Eq. (47), it is readily seen that once the momentum-resolved rf spectroscopy is measured with high resolution, it is possible to determine precisely $s_{\mathbf{q}+}^2$ and $s_{\mathbf{q}-}^2$ and then reconstruct the two-body wave function of spin-orbit bound molecules.

E. Numerical results and discussions

For equal Rashba and Dresselhaus spin-orbit coupling, the bound molecular state exists only on the BEC side of Feshbach resonances with a positive s-wave scattering length, $a_s > 0$ [24]. Thus, it is convenient to take the characteristic binding energy $E_B = \hbar^2/(ma_s^2)$ as the unit for energy and frequency. For the wave vector, we use $k_R = m\lambda/\hbar^2$ as the unit. The strength of spin-orbit coupling may be measured by the ratio

$$\frac{E_\lambda}{E_B} = \left[\frac{\hbar^2}{m\lambda a_s}\right]^{-2}, \tag{49}$$

where we have defined the characteristic spin-orbit energy $E_\lambda \equiv m\lambda^2/\hbar^2 = \hbar^2 k_R^2/m$. Note that, the spin-orbit coupling is also controlled by the effective Zeeman field $h = \Omega_R/2$.

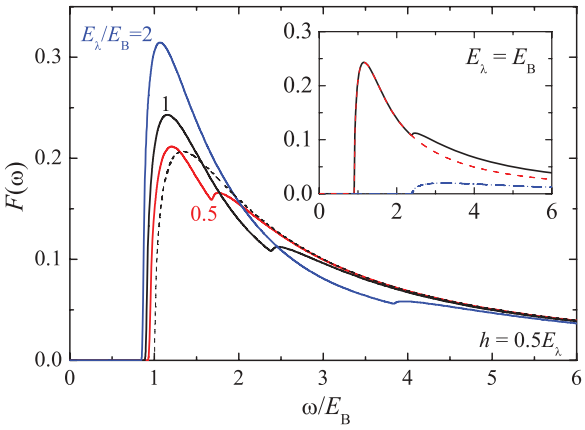

FIG. 1. (Color online) Franck-Condon factor of weakly bound molecules formed by equal Rashba and Dresselhaus spin-orbit coupling, in units of E_B^{-1}. Here we take $h = E_\lambda/2$ or $\Omega_R = \hbar^2 k_R^2/m$ and set $E_\lambda/E_B = 0.5$, 1, and 2. The result without spin-orbit coupling is plotted by the thin dashed line. The inset shows the different contribution from the two final states at $E_\lambda/E_B = 1$. The one with a remaining atom in the lower (upper) helicity branch is plotted by the dashed (dot-dashed) line.

In particular, in the limit of zero Zeeman field $\Omega_R = 0$, there is no spin-orbit coupling term as shown in the original Hamiltonian equation (3), although the characteristic spin-orbit energy $E_\lambda \neq 0$. Using k_R and E_B as the units for wave vector and energy, we can write a set of dimensionless equations for the binding energy $\epsilon_B = -E_0$, normalization factor $\mathcal{C}$, Franck-Condon factor $F(\omega)$, and the momentum-resolved Franck-Condon factor $F(\omega,k_x)$. We then solve them for given parameters E_λ/E_B and h/E_λ. In accord with the normalization condition $\int_{-\infty}^{+\infty} F(\omega) = 1$, the units for $F(\omega)$ and $F(k_x,\omega)$ are taken to be $1/E_B$ and $1/(E_B k_R)$, respectively.

Figure 1 displays the Franck-Condon factor as a function of the rf frequency at $h/E_\lambda = 0.5$ and at several ratios of E_λ/E_B as indicated. For comparison, we show also the rf lineshape without spin-orbit coupling [33], $F(\omega) = (2/\pi)\sqrt{\omega - E_B}/\omega^2$, by the thin dashed line. In the presence of spin-orbit coupling, the existence of two possible final states is clearly revealed by the two peaks in the rf spectra. This is highlighted in the inset for $E_\lambda/E_B = 1$, where the contribution from the two possible final states is plotted separately. The main rf response is from the final state with the remaining atom staying in the lower helicity branch, i.e., the second term in the Franck-Condon factor equation (44). The two peak positions may be roughly estimated from Eq. (48) for the threshold frequency $\omega_{c\pm}$ of two branches,

$$\hbar\omega_{c\pm} = \epsilon_B + \left[\frac{\hbar^2\left(k_R^2 + q_x^2 + q_x k_R\right)}{m} \pm \sqrt{h^2+\lambda^2 q_x^2}\right]_{\min}. \tag{50}$$

With increasing spin-orbit coupling, the low-frequency peak becomes more and more pronounced and shifts slightly towards lower energy. In contrast, the high-frequency peak has a rapid blueshift.

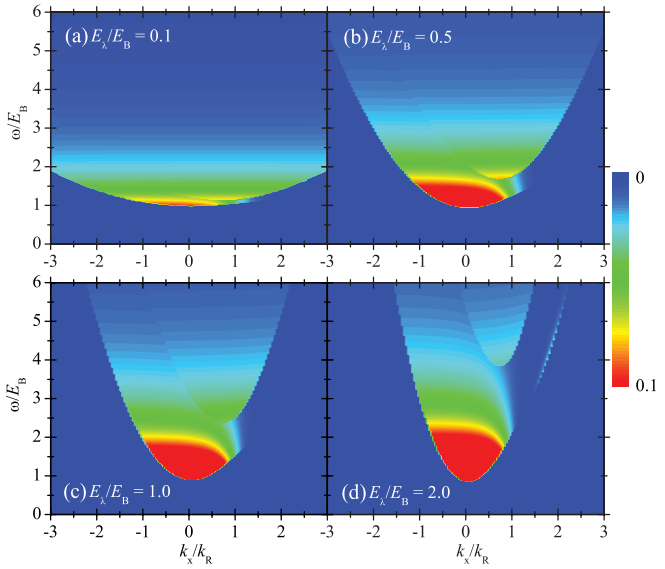

FIG. 2. (Color online) Linear contour plot of momentum-resolved Franck-Condon factor, in units of $(E_B k_R)^{-1}$. Here we take $h = E_\lambda/2$ and consider $E_\lambda/E_B = 0.1$, 0.5, 1, and 2.

Figure 2 presents the corresponding momentum-resolved Franck-Condon factor. We find a strong asymmetric distribution as a function of the momentum k_x. In particular, the contribution from two final states are well separated in different frequency domains and therefore should be easily observed experimentally. The asymmetric distribution of $F(k_x,\omega)$ is mostly evident in energy distribution curve, as shown in Fig. 3, where we plot $F(k_x,\omega)$ as a function of k_x at several given frequencies ω. In the experiment, each of these energy distribution curves can be obtained by a single-shot measurement.

We finally discuss the effect of the effective Zeeman field $h = \Omega_R/2$. Figure 4 shows how the line shape of Franck-Condon factor evolves as a function of the Zeeman field at $E_\lambda/E_B = 1$. In general, the larger the Zeeman field, the stronger the spin-orbit coupling. Therefore, the same as in

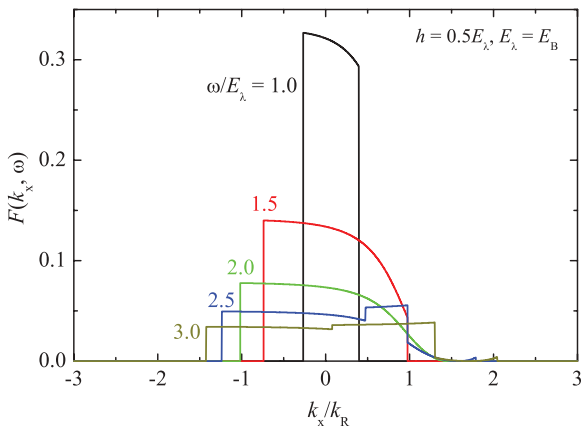

FIG. 3. (Color online) Energy distribution curve of the momentum-resolved Franck-Condon factor, in units of $(E_B k_R)^{-1}$. We consider several values of the rf frequency ω as indicated, under given parameters $h = E_\lambda/2$ and $E_\lambda = E_B$.

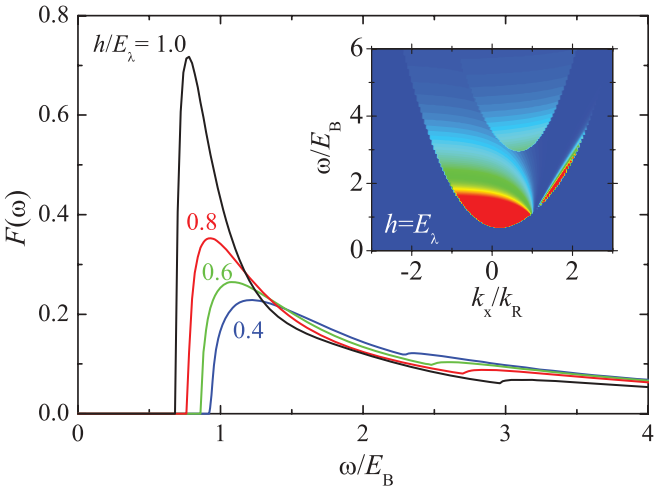

FIG. 4. (Color online) Zeeman-field dependence of the Franck-Condon factor at $E_\lambda = E_B$. Here we vary the effective Zeeman fields $h/E_\lambda = 0.4$, 0.6, 0.8, and 1.0. The inset shows the momentum-resolved Franck-Condon factor at $h = E_\lambda$.

Fig. 1, the increase in Zeeman field leads to a pronounced peak at about the binding energy. There is a redshift in the peak position as the binding energy becomes smaller as the Zeeman field increases. As anticipated, the larger the Zeeman field, the more asymmetric $F(k_x,\omega)$ becomes. In the inset, we show as an example the contour plot of $F(k_x,\omega)$ at $h/E_\lambda = 1$.

IV. RASHBA SPIN-ORBIT COUPLING

We now turn to the case with pure Rashba spin-orbit coupling $\lambda(k_y\sigma_x - k_x\sigma_y)$, which may be realized experimentally in the near future. The single-particle Hamiltonian may be written as [23]

$$\mathcal{H}_0 = \int d\mathbf{r}[\psi_\uparrow^\dagger(\mathbf{r}),\psi_\downarrow^\dagger(\mathbf{r})]\mathcal{S}\begin{bmatrix}\psi_\uparrow(\mathbf{r})\\ \psi_\downarrow(\mathbf{r})\end{bmatrix}, \tag{51}$$

where the matrix

$$\mathcal{S} = \begin{bmatrix}\hbar^2\left(k_R^2+k^2\right)/(2m) & i\lambda\left(k_x - ik_y\right)\\ -i\lambda(k_x+ik_y) & \hbar^2\left(k_R^2+k^2\right)/(2m)\end{bmatrix}. \tag{52}$$

Here λ is the coupling strength of Rashba spin-orbit coupling $k_R \equiv m\lambda/\hbar^2$, and we have added a constant term $\hbar^2 k_R^2/(2m)$ to make the minimum single-particle energy zero [24], i.e., $E_{\min} = 0$.

A. Single-particle solution

We diagonalize the matrix $\mathcal{S}$ to obtain two helicity eigenvalues [23],

$$E_{\mathbf{k}\pm} = \frac{\hbar^2\left(k_R^2+k^2\right)}{2m} \pm \lambda k_\perp, \tag{53}$$

where $k_\perp \equiv \sqrt{k_x^2+k_y^2}$ and "±" stands for the two helicity branches. For later reference, the field operators in the original

spin basis and in the helicity basis are related by

$$c^\dagger_{\mathbf{k}\uparrow} = \frac{1}{\sqrt{2}}(c^\dagger_{\mathbf{k}+} + ie^{i\varphi_{\mathbf{k}}}c^\dagger_{\mathbf{k}-}), \tag{54}$$

$$c^\dagger_{\mathbf{k}\downarrow} = \frac{1}{\sqrt{2}}(ie^{-i\varphi_{\mathbf{k}}}c^\dagger_{\mathbf{k}+} + c^\dagger_{\mathbf{k}-}). \tag{55}$$

Here $\varphi_{\mathbf{k}} \equiv \arg(k_x, k_y)$ is the azimuthal angle of the wave vector $\mathbf{k}_\perp$ in the x-y plane.

B. The initial two-particle bound state $|\Phi_{2B}\rangle$

In the case of Rashba spin-orbit coupling, the two-body wave function can still be written in the same form as in the previous case, i.e., Eq. (22), as shown by Yu and Zhai [22]. The two-body Schrödinger equation leads to [22]

$$A_{\mathbf{k}}\psi_{\uparrow\downarrow}(\mathbf{k}) = +\frac{U_0}{2}\sum_{\mathbf{k}'}[\psi_{\uparrow\downarrow}(\mathbf{k}') - \psi_{\downarrow\uparrow}(\mathbf{k}')] - \lambda(k_y - ik_x)\psi_{\uparrow\uparrow}(\mathbf{k}) + \lambda(k_y + ik_x)\psi_{\downarrow\downarrow}(\mathbf{k}), \tag{56}$$

$$A_{\mathbf{k}}\psi_{\downarrow\uparrow}(\mathbf{k}) = -\frac{U_0}{2}\sum_{\mathbf{k}'}[\psi_{\uparrow\downarrow}(\mathbf{k}') - \psi_{\downarrow\uparrow}(\mathbf{k}')] + \lambda(k_y - ik_x)\psi_{\uparrow\uparrow}(\mathbf{k}) - \lambda(k_y + ik_x)\psi_{\downarrow\downarrow}(\mathbf{k}), \tag{57}$$

$$A_{\mathbf{k}}\psi_{\uparrow\uparrow}(\mathbf{k}) = -\lambda(k_y + ik_x)\psi_{\uparrow\downarrow}(\mathbf{k}) + \lambda(k_y + ik_x)\psi_{\downarrow\uparrow}(\mathbf{k}), \tag{58}$$

$$A_{\mathbf{k}}\psi_{\downarrow\downarrow}(\mathbf{k}) = +\lambda(k_y - ik_x)\psi_{\uparrow\downarrow}(\mathbf{k}) - \lambda(k_y - ik_x)\psi_{\downarrow\uparrow}(\mathbf{k}), \tag{59}$$

where $A_{\mathbf{k}} \equiv E_0 - (\hbar^2 k_R^2/m + \hbar^2 k^2/m) < 0$. It is easy to show that $\psi_a(\mathbf{k}) = 0$ and

$$\left[A_{\mathbf{k}} - \frac{4\lambda^2 k_\perp^2}{A_{\mathbf{k}}}\right]\psi_s(\mathbf{k}) = U_0\sum_{\mathbf{k}'}\psi_s(\mathbf{k}'). \tag{60}$$

Thus, we obtain the (un-normalized) wave function

$$\psi_s(\mathbf{k}) = \frac{1}{2}\left[\frac{1}{E_0 - 2E_{\mathbf{k}+}} + \frac{1}{E_0 - 2E_{\mathbf{k}-}}\right], \tag{61}$$

and the equation for the energy E_0,

$$\frac{m}{4\pi\hbar^2 a_s} = \sum_{\mathbf{k}}\left[\frac{1/2}{E_0 - 2E_{\mathbf{k}+}} + \frac{1/2}{E_0 - 2E_{\mathbf{k}-}} + \frac{m}{\hbar^2 k^2}\right]. \tag{62}$$

The spin-triplet wave functions $\psi_{\uparrow\uparrow}(\mathbf{k})$ and $\psi_{\downarrow\downarrow}(\mathbf{k})$ are given by

$$\psi_{\uparrow\uparrow}(\mathbf{k}) = \left[-ie^{-i\varphi_{\mathbf{k}}}\frac{\sqrt{2}\lambda k_\perp}{E_0 - 2\epsilon_{\mathbf{k}}}\right]\psi_s(\mathbf{k}), \tag{63}$$

$$\psi_{\downarrow\downarrow}(\mathbf{k}) = \left[-ie^{+i\varphi_{\mathbf{k}}}\frac{\sqrt{2}\lambda k_\perp}{E_0 - 2\epsilon_{\mathbf{k}}}\right]\psi_s(\mathbf{k}), \tag{64}$$

where $\epsilon_{\mathbf{k}} \equiv \hbar^2 k^2/(2m)$. The normalization factor for the two-body wave function is therefore

$$\mathcal{C} = \sum_{\mathbf{k}}|\psi_s(\mathbf{k})|^2\left[1 + \frac{4\lambda^2 k_\perp^2}{(E_0 - 2\epsilon_{\mathbf{k}})^2}\right]. \tag{65}$$

C. The final two-particle state $|\Phi_f\rangle$

To obtain the final state, we consider again $\mathcal{V}_{\rm rf}|\Phi_{2B}\rangle$. In the present case, we assume that the rf Hamiltonian is given by

$$\mathcal{V}_{\rm rf} = V_0\sum_{\mathbf{q}}(c^\dagger_{\mathbf{q}3}c_{\mathbf{q}\downarrow} + c^\dagger_{\mathbf{q}\downarrow}c_{\mathbf{q}3}). \tag{66}$$

Following the same procedure as in the case of equal Rashba and Dresselhaus coupling, it is straightforward to show that

$$\mathcal{V}_{\rm rf}|\Phi_{2B}\rangle = -\sqrt{\frac{1}{\mathcal{C}}}V_0\sum_{\mathbf{q}}c^\dagger_{-\mathbf{q}3}[\psi_s(\mathbf{q})c^\dagger_{\mathbf{q}\uparrow} + \sqrt{2}\psi_{\downarrow\downarrow}(\mathbf{q})c^\dagger_{\mathbf{q}\downarrow}]|\text{vac}\rangle. \tag{67}$$

Using Eqs. (54) and (55) to rewrite $c^\dagger_{\mathbf{q}\uparrow}$ and $c^\dagger_{\mathbf{q}\downarrow}$ in terms of $c^\dagger_{\mathbf{q}+}$ and $c^\dagger_{\mathbf{q}-}$, we obtain

$$\mathcal{V}_{\rm rf}|\Phi_{2B}\rangle = -\sqrt{\frac{1}{2\mathcal{C}}}V_0\sum_{\mathbf{q}}\left[\frac{c^\dagger_{-\mathbf{q}3}c^\dagger_{\mathbf{q}+}}{E_0 - 2E_{\mathbf{q}+}} + \frac{ie^{i\varphi_{\mathbf{q}}}c^\dagger_{-\mathbf{q}3}c^\dagger_{\mathbf{q}-}}{E_0 - 2E_{\mathbf{q}-}}\right]|\text{vac}\rangle. \tag{68}$$

Therefore, we have again two final states, differing in the helicity branch that the remaining atom stays. The remaining atom stays in the upper branch with probability $(2\mathcal{C})^{-1}(E_0 - 2E_{\mathbf{q}+})^{-2}$, and in the lower branch with probability $(2\mathcal{C})^{-1}(E_0 - 2E_{\mathbf{q}-})^{-2}$.

D. Momentum-resolved rf spectroscopy

Using Fermi's golden rule, we have immediately the Franck-Condon factor

$$F(\omega) = \frac{1}{\mathcal{C}}\sum_{\mathbf{k}}\left[\frac{\delta(\omega - \mathcal{E}_{\mathbf{k}+}/\hbar)}{2(\epsilon_B + 2E_{\mathbf{k}+})^2} + \frac{\delta(\omega - \mathcal{E}_{\mathbf{k}-}/\hbar)}{2(\epsilon_B + 2E_{\mathbf{k}-})^2}\right], \tag{69}$$

where

$$\mathcal{E}_{\mathbf{k}\pm} \equiv \epsilon_B + \frac{\hbar^2 k_R^2}{2m} + \frac{\hbar^2 k^2}{m} \pm \lambda k_\perp. \tag{70}$$

For Rashba spin-orbit coupling, it is reasonable to define the following momentum-resolved Franck-Condon factor:

$$F(k_\perp,\omega) = \frac{1}{\mathcal{C}} \sum_{k_z} \left[\frac{\delta(\omega - \mathcal{E}_{\mathbf{k}+}/\hbar)}{2(\epsilon_B + 2E_{\mathbf{k}+})^2} + \frac{\delta(\omega - \mathcal{E}_{\mathbf{k}-}/\hbar)}{2(\epsilon_B + 2E_{\mathbf{k}-})^2} \right], \tag{71}$$

where we have summed over the momentum k_z. Integrating over k_z with the help of the two Dirac δ functions, we find that

$$F(k_\perp,\omega) = \frac{m}{16\pi^3\hbar\mathcal{C}} \left[\frac{\Theta(k_{z+}^2)}{(\hbar\omega + \hbar^2 k_R^2/2m + \lambda k_\perp)^2 k_{z+}} + \frac{\Theta(k_{z-}^2)}{(\hbar\omega + \hbar^2 k_R^2/2m - \lambda k_\perp)^2 k_{z-}} \right], \tag{72}$$

where

$$k_{z\pm}^2 = \frac{m}{\hbar}\left(\omega - \frac{\epsilon_B}{\hbar}\right) - \left(\frac{k_R^2}{2} + k_\perp^2 \pm k_R k_\perp\right). \tag{73}$$

It is easy to see that the threshold frequencies for the two final states are given by

$$\hbar\omega_{c+} = \epsilon_B + \frac{\hbar^2 k_R^2}{2m}, \tag{74}$$

$$\hbar\omega_{c-} = \epsilon_B + \frac{\hbar^2 k_R^2}{4m}, \tag{75}$$

which differ by an amount of $\hbar^2 k_R^2/(4m) = E_\lambda/4$. Near ω_{c-}, we find approximately that $F(\omega) \propto \Theta(\omega - \omega_{c-})/\omega^2$. Thus, the line shape near the threshold is similar to that of a two-dimensional (2D) Fermi gas [36]. This similarity is related to the fact that at low energy a three-dimensional (3D) Fermi gas with Rashba spin-orbit coupling has exactly the same density of states as a 2D Fermi gas [14].

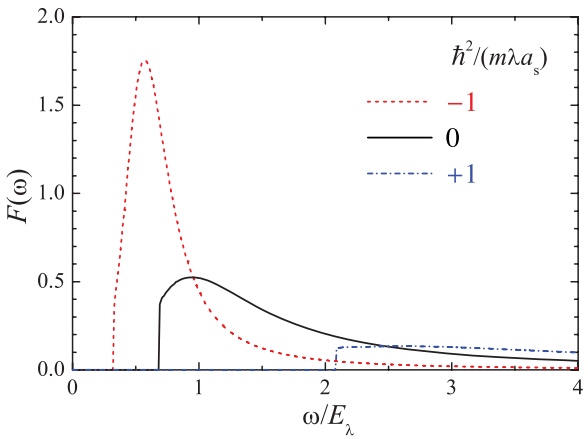

FIG. 5. (Color online) Franck-Condon factor of weakly bound molecules formed by Rashba spin-orbit coupling, in units of E_λ^{-1}. Here we take $\hbar^2/(m\lambda a_s) = -1$ (dashed line), 0 (solid line), and 1 (dot-dashed line). In the deep BCS limit, $\hbar^2/(m\lambda a_s) \to -\infty$, the Franck-Condon factor peaks sharply at $\hbar\omega \simeq E_\lambda/2$ and becomes a δ-like distribution.

E. Numerical results and discussions

For the pure Rashba spin-orbit coupling, the molecular bound state exists for arbitrary s-wave scattering length a_s [19,22,23]. We shall take $k_R = m\lambda/\hbar^2$ and $E_\lambda \equiv m\lambda^2/\hbar^2$ as the units for wave vector and energy, respectively. With

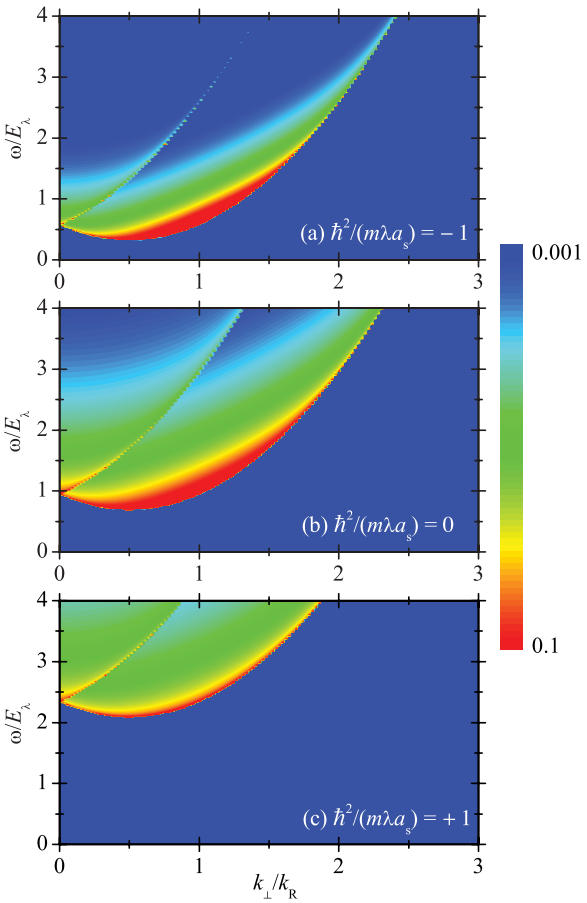

FIG. 6. (Color online) Contour plot of momentum-resolved Franck-Condon factor of weakly bound molecules formed by Rashba spin-orbit coupling, in units of $(E_\lambda k_R)^{-1}$. The intensity increases from blue to red in a logarithmic scale. We consider $\hbar^2/(m\lambda a_s) = -1$ (a), 0 (b), and 1 (c).

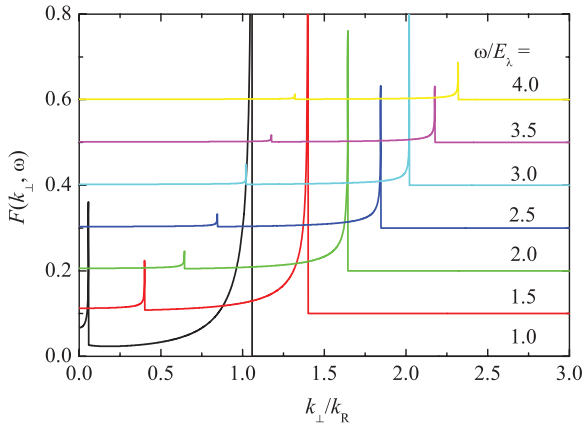

FIG. 7. (Color online) Momentum-resolved Franck-Condon factor of Rashba molecules at $\hbar^2/(m\lambda a_s) = 0$, shown in the form of energy distribution curves at several rf frequencies as indicated.

these units, the dimensionless interaction strength is given by $\hbar^2/(m\lambda a_s)$. The spin-orbit effect should be mostly significant on the BCS side with $\hbar^2/(m\lambda a_s) < 0$, where the bound state cannot exist without spin-orbit coupling.

Figure 5 shows the Franck-Condon factor at three different interaction strengths $\hbar^2/(m\lambda a_s) = -1$, 0, and $+1$. The strong response in the BCS regime ($a_s < 0$) or in the unitary limit ($a_s \to \pm\infty$) is an unambiguous signal of the existence of Rashba molecules. In particular, the rf line shape in the BCS regime shows a sharp peak at about $\hbar\omega \simeq E_\lambda/2$ and decays very fast at high frequency.

In Fig. 6, we present the corresponding momentum-resolved Franck-Condon factor $F(k_\perp,\omega)$, in the form of contour plots. We can see clearly the different response from the two final states. The momentum-resolved rf spectroscopy is particularly useful to identify the contribution from the final state that has a remaining atom in the upper branch, which, being integrated over $k_\perp$, becomes too weak to be resolved in the total rf spectroscopy. Finally, we report in Fig. 7 energy distribution curves of $F(k_\perp,\omega)$ in the unitary limit $\hbar^2/(m\lambda a_s) = 0$. We find two sharp peaks in each energy distribution curve, arising from the two final states. When measured experimentally, these sharp peaks would become much broader owing to the finite experimental energy resolution.

V. CONCLUSIONS

In conclusion, we have investigated theoretically the radio-frequency spectroscopy of weakly bound molecules in a spin-orbit-coupled atomic Fermi gas. The wave function of these molecules is greatly affected by spin-orbit coupling and has both spin-singlet and spin-triplet components. As a result, the line shape of the total radio-frequency spectroscopy is qualitatively different from that of the conventional molecules at the BEC-BCS crossover without spin-orbit coupling. In addition, the momentum-resolved radio frequency becomes highly asymmetric as a function of the momentum. These features are easily observable in current experiments with spin-orbit-coupled Fermi gases of ^{40}K atoms and ^{6}Li atoms. On the other hand, from the high-resolution momentum-resolved radio frequency, we may reconstruct the two-body wave function of the bound molecules.

At finite temperatures, the contribution from atoms to the radio-frequency spectroscopy becomes important. Thus, we may have to treat atoms and weakly bound molecules on an equal footing. A more in-depth investigation of spectroscopy requires complicated many-body calculations beyond our simple two-body picture pursued in the present work [39,40]. At the Fermi degenerate temperature T_F, which is the typical temperature scale for the recently realized spin-orbit atomic Fermi gas [4,5], we may use a quantum virial expansion method to obtain reliable theoretical predictions [41].

ACKNOWLEDGMENTS

We would like to thank Zeng-Qiang Yu and Hui Zhai for useful discussions. H.H. and X.J.L. are supported by the ARC Discovery Projects (Grant No. DP0984522 and No. DP0984637) and the National Basic Research Program of China (NFRP-China, Grant No. 2011CB921502). H.P. is supported by the NSF and the Welch Foundation (Grant No. C-1669). J.Z. is supported by the NSFC Project for Excellent Research Team (Grant No. 61121064) and the NFRP-China (Grant No. 2011CB921601). S.G.P is supported by the NSFC-China (Grant No. 11004224) and the NFRP-China (Grant No. 2011CB921601).

[1] X.-L. Qi and S.-C. Zhang, Phys. Today **63** (1), 33 (2010).
[2] M. Z. Hasan and C. L. Kane, Rev. Mod. Phys. **82**, 3045 (2010).
[3] Y.-J. Lin, K. Jiménez-García, and I. B. Spielman, Nature (London) **471**, 83 (2011).
[4] P. Wang, Z.-Q. Yu, Z. Fu, J. Miao, L. Huang, S. Chai, H. Zhai, and J. Zhang, Phys. Rev. Lett. **109**, 095301 (2012).
[5] L. W. Cheuk, A. T. Sommer, Z. Hadzibabic, T. Yefsah, W. S. Bakr, and M. W. Zwierlein, Phys. Rev. Lett. **109**, 095302 (2012).
[6] T. D. Stanescu, B. Anderson, and V. Galitski, Phys. Rev. A **78**, 023616 (2008).
[7] J. Larson and E. Sjöqvist, Phys. Rev. A **79**, 043627 (2009).
[8] C. Wang, C. Gao, C.-M. Jian, and H. Zhai, Phys. Rev. Lett. **105**, 160403 (2010).
[9] C. Wu, I. Mondragon-Shem, and X.-F. Zhou, Chin. Phys. Lett. **28**, 097102 (2011).
[10] T.-L. Ho and S. Zhang, Phys. Rev. Lett. **107**, 150403 (2011).
[11] X. Q. Xu and J. H. Han, Phys. Rev. Lett. **107**, 200401 (2011).
[12] S. Sinha, R. Nath, and L. Santos, Phys. Rev. Lett. **107**, 270401 (2011).
[13] H. Hu, B. Ramachandhran, H. Pu, and X.-J. Liu, Phys. Rev. Lett. **108**, 010402 (2012).
[14] H. Hu and X.-J. Liu, Phys. Rev. A **85**, 013619 (2012).
[15] B. Ramachandhran, B. Opanchuk, X.-J. Liu, H. Pu, P. D. Drummond, and H. Hu, Phys. Rev. A **85**, 023606 (2012).
[16] R. Barnett, S. Powell, T. Graß, M. Lewenstein, and S. Das Sarma, Phys. Rev. A **85**, 023615 (2012).

[17] Y. Deng, J. Cheng, H. Jing, C.-P. Sun, and S. Yi, Phys. Rev. Lett. **108**, 125301 (2012).
[18] Q. Zhu, C. Zhang, and B. Wu, arXiv:1109.5811.
[19] J. P. Vyasanakere and V. B. Shenoy, Phys. Rev. B **83**, 094515 (2011).
[20] M. Iskin and A. L. Subaşi, Phys. Rev. Lett. **107**, 050402 (2011).
[21] S. L. Zhu, L. B. Shao, Z. D. Wang, and L. M. Duan, Phys. Rev. Lett. **106**, 100404 (2011).
[22] Z. Q. Yu and H. Zhai, Phys. Rev. Lett. **107**, 195305 (2011).
[23] H. Hu, L. Jiang, X.-J. Liu, and H. Pu, Phys. Rev. Lett. **107**, 195304 (2011).
[24] L. Jiang, X.-J. Liu, H. Hu, and H. Pu, Phys. Rev. A **84**, 063618 (2011).
[25] M. Gong, S. Tewari, and C. Zhang, Phys. Rev. Lett. **107**, 195303 (2011).
[26] L. Han and C. A. R. Sá de Melo, Phys. Rev. A **85**, 011606(R) (2012).
[27] X.-J. Liu, L. Jiang, H. Pu, and H. Hu, Phys. Rev. A **85**, 021603 (2012).
[28] X. Cui, Phys. Rev. A **85**, 022705 (2012).
[29] X.-J. Liu and H. Hu, Phys. Rev. A **85**, 033622 (2012).
[30] L. He and X.-G. Huang, Phys. Rev. Lett. **108**, 145302 (2012).
[31] W. Yi and W. Zhang, Phys. Rev. Lett. **109**, 140402 (2012).
[32] C. Chin, R. Grimm, P. S. Julienne, and E. Tiesinga, Rev. Mod. Phys. **82**, 1225 (2010).
[33] C. Chin and P. S. Julienne, Phys. Rev. A **71**, 012713 (2005).
[34] C. Chin, M. Bartenstein, A. Altmeyer, S. Riedl, S. Jochim, J. Hecker Denschlag, and R. Grimm, Science **305**, 1128 (2004).
[35] C. H. Schunck, Y. Shin, A. Schirotzek, and W. Ketterle, Nature (London) **454**, 739 (2008).
[36] Y. Zhang, W. Ong, I. Arakelyan, and J. E. Thomas, Phys. Rev. Lett. **108**, 235302 (2012).
[37] C. Kohstall, M. Zaccanti, M. Jag, A. Trenkwalder, P. Massignan, G. M. Bruun, F. Schreck, and R. Grimm, Nature (London) **485**, 615 (2012).
[38] M. Koschorreck, D. Pertot, E. Vogt, B. Fröhlich, M. Feld, and M. Köhl, Nature (London) **485**, 619 (2012).
[39] X.-J. Liu and H. Hu, Phys. Rev. A **72**, 063613 (2005).
[40] H. Hu, X.-J. Liu, and P. D. Drummond, Europhys. Lett. **74**, 574 (2006).
[41] H. Hu, X.-J. Liu, P. D. Drummond, and H. Dong, Phys. Rev. Lett. **104**, 240407 (2010).